

Time-Domain Broadband 60 GHz Channel Sounder for Vehicle-to-Vehicle Channel Measurement

Ales Prokes^{*}, Josef Vychodil^{*}, Tomas Mikulasek^{*}, Jiri Blumenstein^{*},
Erich Zöchmann^{†*}, Herbert Groll[‡], Christoph F. Mecklenbräuker[‡],
Markus Hofer^x, David Löschenbrand^x, Laura Bernadó^x
Thomas Zemen^x, Seun Sangodoyin^{††}, Andreas Molisch^{††}

^{*}Department of Radio Electronics, Brno University of Technology, Czech Republic, prokes@vutbr.cz

[†] Christian Doppler Laboratory for Dependable Wireless Connectivity for the Society in Motion

[‡] Institute of Telecommunications, TU Wien, Austria

^x Safety and Security Department, Austrian Institute of Technology, Austria

^{††} Wireless Devices and Systems Group, University of Southern California, USA

Abstract— The paper deals with a time varying vehicle-to-vehicle channel measurement in the 60 GHz millimeter wave (MMW) band using a unique time-domain channel sounder built from off-the-shelf components and standard measurement devices and employing Golay complementary sequences as the excitation signal. The aim of this work is to describe the sounder architecture, primary data processing technique, achievable system parameters, and preliminary measurement results. We measured the signal propagation between two passing vehicles and characterized the signal reflected by a car driving on a highway. The proper operation of the channel sounder is verified by a reference measurement performed with an MMW vector network analyzer in a rugged stationary office environment. The goal of the paper is to show the measurement capability of the sounder and its superior features like 8 GHz measuring bandwidth enabling high time resolution or good dynamic range allowing an analysis of weak multipath components.

Keywords—millimeter wave, channel measurement, channel sounder, channel impulse response

I. INTRODUCTION

Recent societal trends show a continuously increasing demand for high-speed mobile communications. The steadily growing number of communication devices per area and increasing quality of services require the allocation of more frequency resources. The global bandwidth shortage in the recently used frequency bands up to 6 GHz has motivated an exploration of the underutilized millimeter wave (MMW) frequency spectrum. MMW frequencies between 30 and 300 GHz have attracted growing attention as a possible candidate for next-generation cellular networks [1].

Designing any communication systems is impossible without a detailed knowledge of the transmission channel features. Specific limitations of MMW signal propagation, extremely large bandwidth and time-varying environment caused by mobile users connected to backhaul networks and

traveling very often in rugged municipal environments, create unprecedented challenges to the development of broadband communication systems using advanced technologies for eliminating the undesirable time-varying channel features.

Recent works have primarily been aimed at channel analyses and modelling based on real-world measurement in the frequency domain (FD) or time domain (TD). FD sounders are most frequently based on a combination of a generator & a signal/spectrum/network analyzer, which use a continuous wave or a frequency-swept signal for the channel sounding [2], [3]. This type of the FD sounder is limited either to narrowband channels or due to a slow frequency sweep to stationary channels. In contrast the time domain sounders and certain types of FD sounders such as chirp [4] and multitone [5]–[8] allow time-varying broadband channel characterization. TD sounders can be based on an arbitrary waveform generator (AWG) generating an excitation signal in the form of very narrow repetitive impulses (e.g. Gaussian). A coherent detection of the pulses (often converted into in-phase and quadrature components) is possible using a wideband oscilloscope [9], [10]. Although pulse sounding systems are limited by high sensitivity to noise and interference due to the large peak-to-average-power ratio (PAPR) penalty [11], they are not very frequently used. Probably the most popular technique for channel sounding uses a time-based spread spectrum approach, where a wideband pseudorandom binary sequence (PRBS) transmitted through the channel is correlated at the receiver with an identical PRBS code [12]–[15]. Such *correlative* sounders exploit a constant signal envelope, which allows obtaining very good power efficiency, and further they exhibit a correlation gain, which extends the system dynamic range. Some drawback of such a concept is the longer measuring time. A special sub-category of PRBS-based systems is made up of “sliding” sounders. The correlation of the PRBS code is performed at a slightly offset bit rate that allows the received PRBS to “slide” past the slower sequence [16].

Note that choosing the appropriate PRBS for the channel sounding is very important. For example, the maximal length binary sequences (known as the M -sequences) have very good correlation properties (almost zero periodic correlation except for the peak) and, due to their periodicity, also minimal leakage effects caused by FFT [14]. Golay complementary sequences have similar properties and, moreover, they exhibit a great ability to mitigate unwanted nonlinearity effects produced by channel sounder analog circuits [17].

All the above sounders require some kind of receiver and transmitter synchronization. In the case of measurement at a shorter distance the synchronization is provided most frequently by 10 MHz reference or by a similar constant frequency signal [2], [3], [6]–[8], [10], and [13]–[16]. Note that some sounders use also a triggering signal to tell the receiver when the excitation signal is being transmitted. Longer measuring distances require a different approach. Time domain sounders generating narrow pulses can be triggered internally by the first received pulse [9]. Another synchronization technique uses two GPS disciplined oscillators or rubidium clocks which are installed separately in the receiving and transmitting sections [5], [12].

A comprehensive survey of channel sounders operating at frequencies above 3 GHz is presented in [11]. This study compares over 40 sounders, of which more than 20 works in the MMW band, in terms of carrier frequency, synchronization methods, bandwidth, and other features.

The main contributions of this paper are:

- Introduction of a new concept of time-domain broadband correlative MMW channel sounder built from off-the-shelf components and standard measurement devices, whose correct operation is demonstrated by a reference measurement.
- Presentation of original preliminary results of measurements aimed at the signal propagation between two passing cars and at the signal reflection by a car driving on a highway.

The new design of the sounder was motivated by the need to measure signal propagation, firstly inside a moving car [13] and then between vehicles. Although there are a number of various time-domain channel sounders published in the available literature, we have chosen our own concept which does not require any circuit design, is based on measurement devices available at our workplace (which significantly accelerated sounder realization and reduced total costs), and offers very good parameters, especially with respect to bandwidth, which is, according to our best knowledge, the largest among the published sounders. The large bandwidth is advantageous in small rugged environment (such as a car cabin) as it exhibits excellent time resolution of multipath components (MPCs).

The results are presented without any detailed analyses. The aim of the paper is to show the measurement capability of the channel sounder and to inspire interested workers in the field to realize broadband time-varying MMW channel measurements.

The rest of the paper is organized as follows. Section 2 describes the channel sounder architecture and the principle of operation, and gives a list of the fundamental parameters. Section 3 briefly informs about the techniques of signal processing used for the channel impulse response (CIR) calculation. Section 4 deals with the verification of the measured CIR with a reference obtained using a vector network analyzer (VNA). Then in Section 5, the real-world measurement results are shown. A summary of the paper is given in the conclusion.

II. MEASUREMENT SETUP

The time-domain channel sounder, whose concept is based on [13], is composed of a transmitter (TX) and a receiver (RX). The transmitter depicted in Fig. 1 is based on an Anritsu MP1800A Signal Quality Analyzer (working as a PRBS generator), whose output baseband signal is upconverted into the MMW band using a SiversIma FC1005V/00 V-band up/down converter equipped with programmable PLL local oscillators [18]. To enhance the phase noise performance, the oscillators are disconnected and the reference signal for up-conversion is applied from an Agilent E8257B frequency-stable, low phase-noise generator. The low pass filter (LPF) is optional and limits, together with the internal up/down converter filter, the frequency band of PRBS. For mobile operation, the transmitter is supplied from an uninterruptible power supply DELL 5600W 4U 230V. The receiver in Fig. 2 is created using a Tektronix MSO72004C (20 GHz, 50 GS/s) Mixed Signal Oscilloscope, a SiversIma FC1003V/01 V-band up/down converter (without local oscillators) changing the frequency from the MMW band to the baseband, and a carrier generator Agilent 83752A. Downloading data from the oscilloscope, their basic processing, and setting the oscilloscope parameters are controlled by LabView.

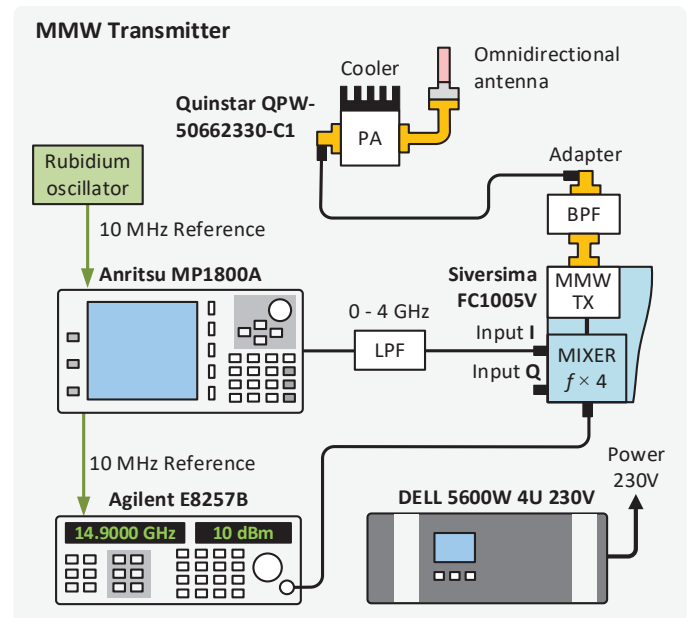


Fig. 1. Block diagram of the channel sounder TX part.

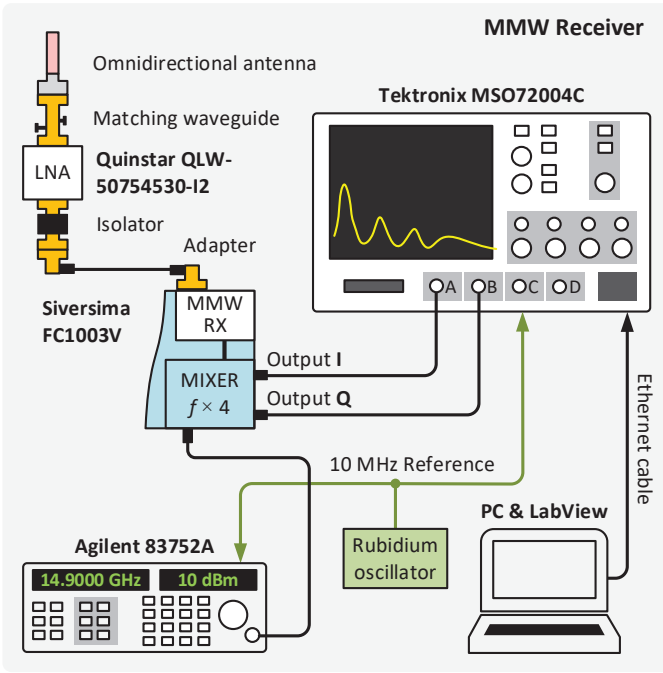


Fig. 2. Block diagram of the channel sounder RX part.

To compensate for large propagation loss in the MMW band and an attenuation in coaxial cables, the Quinstar QLW-50754530-I2 low noise amplifier (LNA) and QPW-50662330-C1 power amplifier (PA) are used. To achieve synchronization between transmitter and receiver both the channel sounder parts are supplied with a 10 MHz reference frequency generated by the Rubidium LPRO 10MHz Oscillators [19].

The operation of the testbed is straightforward. A seamless repeating signal based on the Golay complementary sequences at the data rate $R_{PS} = 12.5$ Gbit/s is frequency limited to the 0 – 4 GHz bandwidth and up-converted into the MMW band with center frequency of 59.6 GHz. A band-pass filter (BPF) partially suppresses the leakage of the local oscillator signal into the RF path to prevent PA saturation. Finally, the signal is fed into the power amplifier with a gain of 35 ± 3 dB through a coaxial cable with an attenuation of 12 dB.

The output powers of the PRBS and reference signal generators are 5 dBm and 10 dBm respectively. In this case the MMW signal is transmitted and received using the omnidirectional SIW slot antennas [20]. The received signal then passes through the LNA with a gain of 33 ± 3 dB and a noise figure of 4.5 dB and through the coaxial cable with an attenuation of 12 dB. To suppress the front-end oscillations caused by the large gain of the amplifier and the following Siversima input circuits, a waveguide isolator and a special waveguide tuner with three screws working as a matching circuit are used. The quadrature down-conversion mixer produces two baseband signals, I and Q, which are digitized and stored in the internal memory of the oscilloscope working as a matched receiver. Because the converter includes the frequency multiplier by a factor of 4, the generator output frequency is set to 14.9 GHz.

The Golay sequences [21] are employed as the excitation signal due to their very good circular correlation properties, which invoke using a very convenient circular auto-correlation technique for the CIR calculation. The length of one sequence defines the maximum observable time span $T_{max} = N_b/R_{PS}$. For the chosen $k = 11$ we get $N_b = 2048$ and $T_{max} = 163.8$ ns. Assuming the speed of light $c = 3 \times 10^8$ m/s we can obtain the maximum observable distance $L_{max} = 49.15$ m. The Golay complementary sequences have also convenient properties when non-linear components are used in the measurement chain as mentioned above and described in [17]. Selected system parameters are summarized in Table 1 (see also Section III).

In order to suppress the oscilloscope wideband noise and down-converter LO leakage, we use a built-in 5 GHz user-selectable bandwidth limit filter. This option can only be used when the full sampling rate is chosen. Considering the memory depth of the oscilloscope $M_D = 31.25$ Msa per channel, the full sampling rate $R_S = 50$ GS/s, and the time span $T_{max} = 163.8$ ns we can calculate important system parameters such as the number of samples per CIR, number of saved CIRs, and total measurement time. To ensure sufficient measurement time, we insert the time delay $T_D = 0.82$ ms, 4.915 ms, or 9.83 ms between two subsequently saved CIRs. Because the maximum of 468 CIRs can be stored in the oscilloscope memory, the above sampling period allow us to analyze the channel within the time interval of $T_M = 0.3$ s, 2.3 s, or 4.6 s. The above time delays, which are controlled by the oscilloscope, are chosen to obtain simplified receiver synchronization, for which T_D is calculated as a least common multiplier of the 10 MHz reference signal period and total length of single or multiple sounding sequence ($8 \times T_{max}$). However, to analyze the Doppler spread in a sufficient range, the T_D has to be significantly reduced. Such an improvement is possible, but not trivial. Note that a correlation technique complicates the evaluation of the Doppler shift caused by a moving vehicle. This is because the correlation of a frequency shifted PRBS with its pattern stored in the receiver, does not provide information about shift, but only affects the correlator output signal amplitude. This drawback can be solved for example by a bank of frequency-shifted PRBS patterns used for correlation. Unfortunately, to get reasonable sensitivity to relatively small frequency changes, the measurement bandwidth would have to be narrower or the PRBS would have to be longer. The reduction of T_D is necessary also because no anti-aliasing filter can be applied for image rejection of measured CIR sequences. For additional information about the channel sounder modified for UWB, see [22].

TABLE I. LIST OF SELECTED SYSTEM PARAMETERS

	Relation	Parameter
Number of PRBS bits [-]	$N_b = 2^k$	2048
Maximum observable time [ns]	$T_{max} = N_b/R_{PS}$	163.8
Maximum observable distance [m]	$L_{max} = cT_{max}$	49.13
Number of samples per CIR [-]	$N_{CS} = N_b R_S / R_{PS}$	8192
Number of saved CIRs [-]	$N_{CIR} = M_D / (8 \cdot N_{CS})$	468
Total measurement time [s]	$T_M = N_{CIR} T_D$	0.38 (2.3, 4.6)
Correlation gain [dB]	$G_c = 10 \log(4 \cdot N_{bit})$	39.1

III. SIGNAL PROCESSING TECHNIQUES

Signal processing techniques applied in the channel sounder include acquisition of particular PRBSs, mitigation of the spurs, and calculation of the CIR. Note that the sounder is calibrated before measurement. For this purpose, the receiver and the transmitter are interconnected via an attenuator and then the IQ imbalances are compensated, and the frequency characteristic is flattened. Because these operations are relatively complex, they will be the subject of another paper.

A. Generation of PRBS sequence and mitigation of spurs

Because some blocks of the channel sounder (especially amplifiers and mixers) exhibit nonlinear behavior and produce plenty of spurs, which can significantly decrease the dynamic range [23], the Golay complementary pair marked as $A(t)$, $B(t)$ is combined with the inverted counterparts $-A(t)$ and $-B(t)$ [17]. Each sequence is sent twice to reduce the overlapping ratio of different sequences caused by a multipath propagation. The complete transmit signal is then $[A(t) A(t) -A(t) -A(t) B(t) B(t) -B(t) -B(t)]$, i.e. a recurring sequence of $8 \times N_b$ bits, is used for channel sounding. A received signal composed of several MPCs is up-sampled at the ratio of R_S/R_{PS} and correlated with the $[A(t) -A(t) B(t) -B(t)]$ sequences as shown in Fig. 3. The results of all four correlations are then averaged, which creates a single vector containing $N_{CS} = N_b R_S/R_{PS} = 8192$ samples.

Because we calculate four different cross-correlations, the correlation gain is $G_C \approx 10 \log(4 \cdot N_{bit}) = 39.1$ dB. Since the dynamic range of the MSO72004C oscilloscope in the given frequency band is about 35 dB [24], the theoretical limit of total dynamic range approaches 74 dB. However, the spur mitigation technique based on the Golay complementary sequences is in practice of only limited efficiency, the real dynamic range of the sounder is about 45 dB.

B. Calculation of CIR

Suppose that the measured channel is time invariant for the coherence time, and then changes to a different fading state. Let, further, the time of a single CIR measurement be shorter than the coherence time, then the channel response $h(t, t')$ can be considered as a function of two time variables t and t' , which in the following text denote the sampling time and the measurement time (time of capturing a sequence of CIRs) respectively.

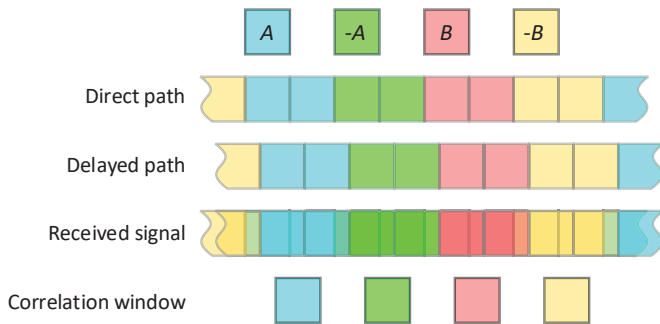


Fig. 3. Forming of received signal from the two time-overlapping components.

To estimate $h(t, t')$, the cross-correlation $R_{xy}(\tau, t')$ between the system input $x(t)$ and the output $y(t)$ may be employed [25]

$$R_{xy}(\tau, t') = h(t, t') * R_{xx}(t), \quad (1)$$

where $R_{xx}(t)$ is the autocorrelation function of the input signal $x(t)$ and $*$ denotes convolution. Because the autocorrelation $R_{xx}(t)$ of the Golay sequence is actually a sharp triangle function, we can write $R_{xx}(t) \approx \delta(t)$, where $\delta(t)$ is the Dirac pulse. Thus, the cross-correlation function is equal to the system impulse response as follows

$$R_{xy}(\tau, t') \approx [h(t, t') * \delta(t)] = h(t, t'). \quad (2)$$

Since the transmitted Golay sequences and their counterparts $x_i(t)$, where $x_1(t) = A(t)$, $x_2(t) = B(t)$, $x_3(t) = -A(t)$ and $x_4(t) = -B(t)$, are known in the receiver, the channel impulse response $h(t, t')$ can be estimated from the corresponding received sequences $y_i(t, t')$ using cross-correlation, and considering further the relation between correlation and convolution [25] the CIR can be finally expressed as

$$h(t, t') = \frac{1}{4} \sum_{i=1}^4 x_i(t) * y_i^*(-t, t'), \quad (3)$$

where y^* is the complex conjugate of y . To accelerate the CIR calculation, equation (3) is transformed from the sampling time domain to the frequency domain and back using the complex (inverse) fast Fourier transform ((I)FFT)

$$h(t, t') = \frac{1}{4} \text{IFFT} \sum_{i=1}^4 \{ \text{FFT}[x_i(t)] \times \text{FFT}[y_i^*(-t, t')] \}. \quad (4)$$

Note that in real calculation the time is discrete i.e. $t = n/R_S$, where $n = \langle 1, N_b \rangle$.

IV. VERIFICATION OF THE MEASURED CIR VIA REFERENCE MEASUREMENT

To verify the measurement accuracy, we performed several measurements in a rugged stationary office environment with the realized channel sounder in the time domain and with a calibrated Rohde & Schwarz ZVA67 VNA in the frequency

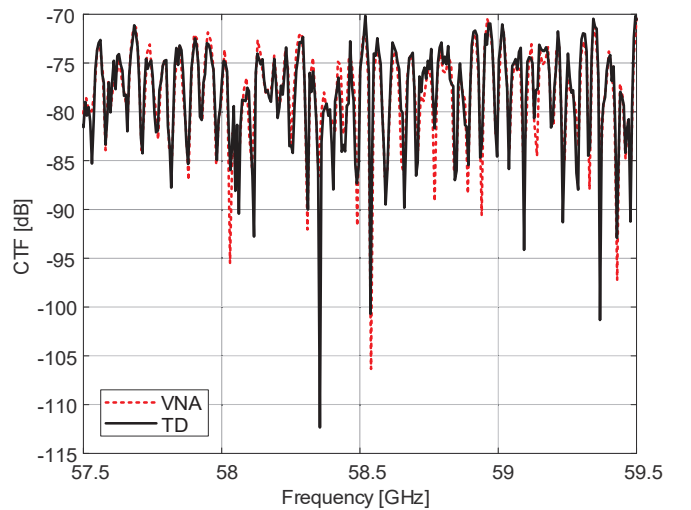


Fig. 4. Comparison of CTFs obtained by the vector network analyzer (VNA) and by the realized sounder (TD).

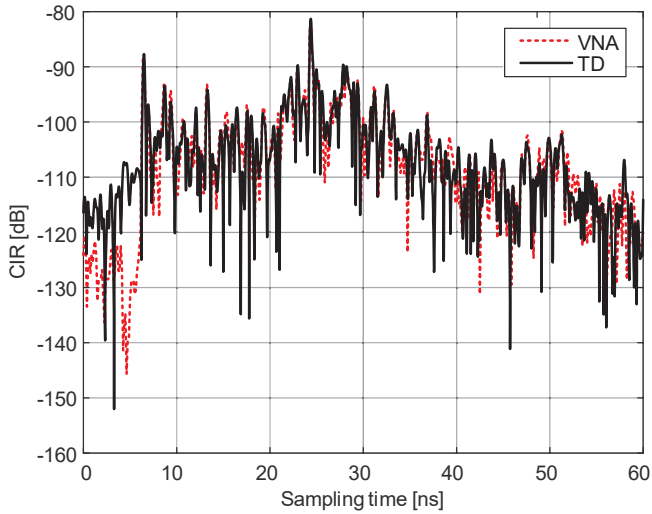


Fig. 5. Comparison of measured CIRs.

domain. The antennas were directed so that there was no LOS component. During the measurements, the antennas were fixed, and the environment was unchanged. The results were compared in both, the time and the frequency domains. Conversion between the two domains was performed using (I)FFT.

An example of the channel transfer functions (CTFs) comparison is shown in Fig. 4. To show the difference between CTFs more clearly, only a 2 GHz bandwidth cutout is shown. More important is the comparison of CIRs in the time domain shown in Fig. 5. It is obvious that there is a good match for both the CTFs and CIRs, especially at a high level of MPCs. Differences at low levels are caused by different intrinsic noise levels of the measurement setups. Because the coaxial cables used are not phase-stable, the measurement results are sensitive to their position and configuration. During the change of one measurement setup to another it is impossible to avoid some manipulation with the cables, which probably contributes to the

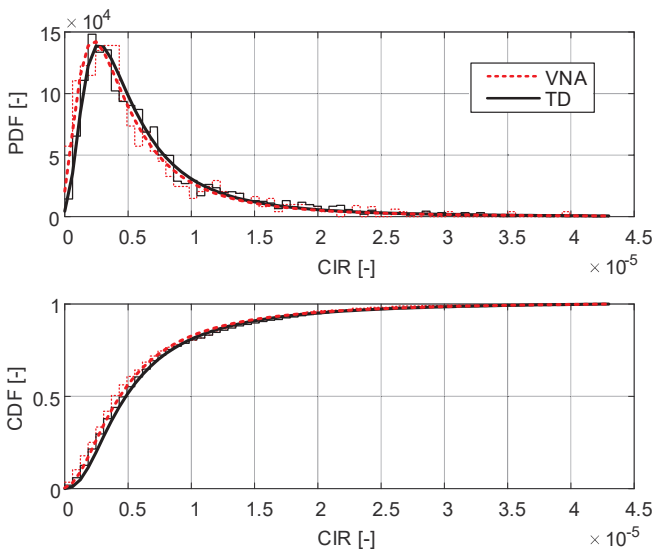


Fig. 6. Comparison of PDF and CDF calculated for CIRs measured in time and frequency domains.



Fig. 7. Testing the channel sounder using two passing cars.

differences also at higher levels of CTFs and CIRs. Other differences (predominantly at the beginning of CIRs) are caused also by the artefacts of FFT calculation.

The probability distribution function (PDF), calculated as a histogram, and the cumulative distribution function (CDF) of the CIRs depicted in Fig. 5 and converted into linear scale inside the interval from 5 to 55 ns and finally fitted by the *generalized extreme value* distribution are shown in Fig. 6. The differences between the CDFs and the PDFs are noticeable particularly at low signal levels, where the effect of the time domain sounder noise is significant.

V. REAL MEASUREMENTS

We tested the channel sounder in two different scenarios. In the first scenario, we measured the CIRs for two passing cars on the road (VW CC 2.0 TDi and Ford Fusion 1.4i) carrying the TX and RX parts of the sounder. The TX part was supplied with the uninterruptible power supply (UPS) as mentioned above, and the RX part from a power station carried on a trailer as shown in Fig. 7. The power station was used because of the large power

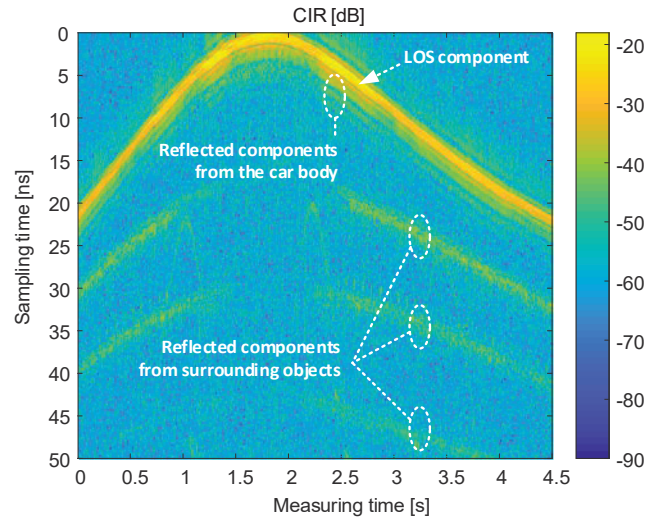


Fig. 8. Example of measured CIR evolving in time for the passing cars.

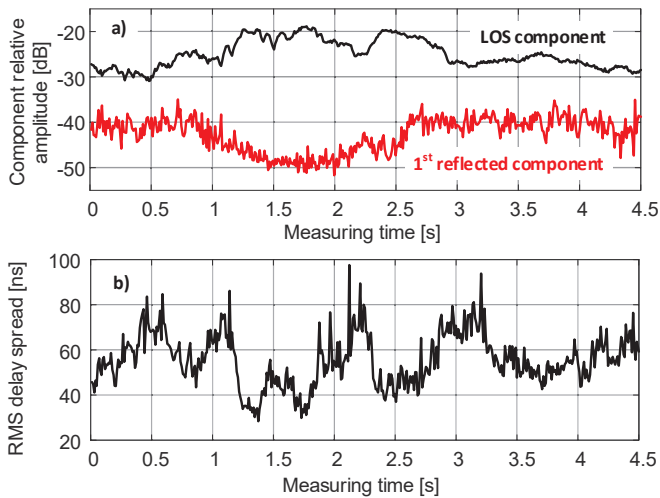


Fig. 9. Relative amplitude of the LOS and reflected component (a) and RMS delay spread (b) in dependence on measuring time.

consumption of the oscilloscope that would discharge an UPS in tens of minutes. The figure also shows details of the RX and TX front-ends mounted on the car roofs. An example of the measured CIR is shown in Fig. 8.

It is obvious that the CIR contains a few MPCs reflected from surrounding objects (street lighting columns, traffic signs and the wall situated on the farther side of the road) and from the car bodies (from roof and hood). While for longer distances between the cars the MPCs are relatively strong, in the case the cars are close together (lowest sampling time), the MPCs reflected from surrounding objects are weaker because the lighting columns and other objects are probably shadowed by the higher Ford Fusion car.

The level of the received signal components in dependence on the mutual position of the cars is also influenced by the radiation characteristics of the SIW slot antennas. Although they are designed as much as possible to be omnidirectional, there is some non-negligible variation in the radiation power from -7 dB to 5 dB (related to the mean value 0 dBi) depending on the frequency and horizontal irradiation angle [20]. The relative amplitudes of the LOS and the first components reflected from



Fig. 10. Testing the channel sounder in “radar mode” on a highway.

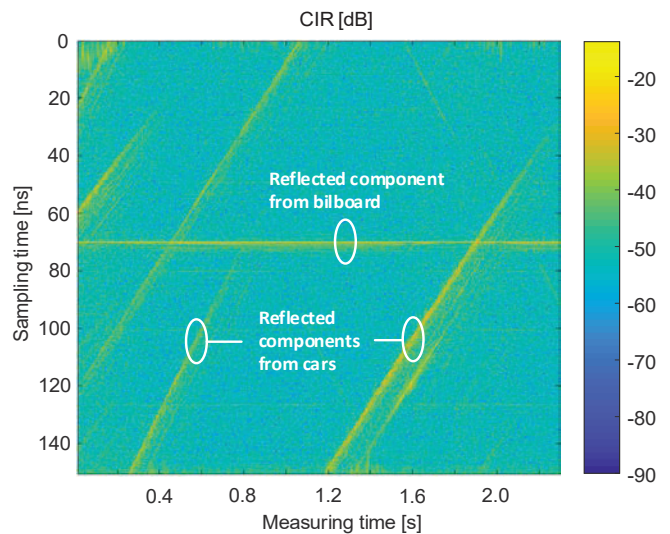


Fig. 11. Example of measured CIRs for cars driving on a highway.

surrounding objects (the first component below the LOS component) calculated as the maximum values for each instant measuring time are shown in Fig. 9 a). The RMS delay spread in dependence on the measuring time is shown in Fig. 9 b). Its relation to the LOS component amplitude in Fig. 9 a) is obvious (the larger the amplitude the smaller the delay spread). Note that the sampling time values are not absolute. The vertical position of all the components depends on the time shift between the periodically generated PRBS and the manual triggering of the oscilloscope.

In the second scenario, the sounder operated as a radar. The TX part was situated on a bridge above the highway and the RX part was mounted on a tripod standing below the bridge on the ground as shown in Fig. 10. To obtain a longer measuring distance (just for the reflected signal) we used a horn antenna (with gain of 24 dBi) on the receiver and an open waveguide (with gain of 6 dBi in the main lobe) on the transmitter.

It is evident from Fig. 11 that the vehicles have multiple reflection surfaces leading to the clustering of the CIR and that

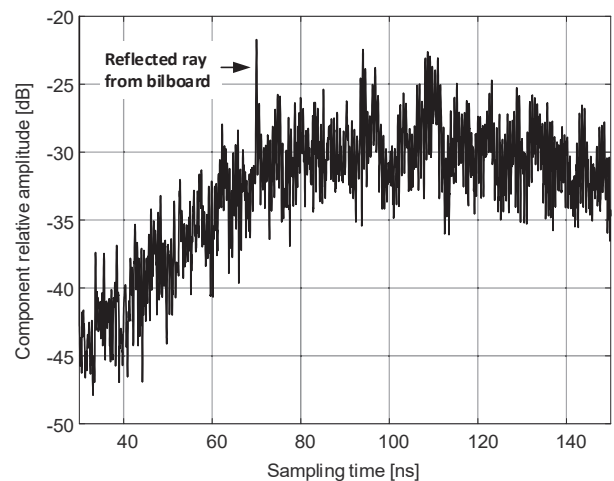


Fig. 12. Relative amplitude of the rightmost marked component from Fig. 11 in dependence on sampling time.

the speeds of vehicles are slightly different. The small-scale variation of the CIR relative amplitude is probably caused by the change of the reflecting area angle related to the antennas while the car is moving and shaking as demonstrated in Fig. 12 on the example of the rightmost marked component in Fig. 11. The reflected peak moves on the sampling time scale from about 30 ns to 150 ns in a measuring time interval of approximately 1 s (from 1.2 to 2.2 s). In other words, the distance of $120 \text{ ns} \times 3e8 \text{ m/s} = 36 \text{ m}$ is overcome during one second which corresponds to a velocity of 129.6 km/h.

VI. CONCLUSION

We propose a MMW channel sounder realized with commercial off the shelf (COTS) components only. It consists entirely of standard measurement devices and common microwave components. The sounder realizes 8 GHz bandwidth, more than 1000 measurements per second, up to a few seconds recording duration, and a satisfactory dynamic range. Its correct operation was verified using reference measurement obtained via VNA.

By analyzing the measured data we have discovered that in the case of vehicle-to-vehicle LOS channels the sounder allows analyzing relatively weak MPCs originating by interacting objects in the propagation environment, and that there is relatively large small-scale variation in the LOS component (even when cars are close to each other) caused probably by imperfect omnidirectional irradiation of the SIW slot antennas. It has also been found that the car driving on a highway exhibits multiple reflection surfaces and that the unavoidable small-scale variation of the LOS component is affected by the movement and shaking of the car.

Recently we have doubled the oscilloscope memory depth and currently are working on an acceleration of the CIR sequence measurement, a development of software for evaluation of the Doppler spread, a more precise description of RF and down-converting blocks, and on an analysis of the measured data.

ACKNOWLEDGMENT

The research described in this paper was financed by the Czech Science Foundation, Project No. 17-27068S, and by the National Sustainability Program under grant LO1401. For the research, the infrastructure of the SIX Center was used. The financial support by the Austrian Federal Ministry for Digital and Economic Affairs is gratefully acknowledged.

REFERENCES

- [1] M. R. Akdeniz et al., "Millimeter wave channel modeling and cellular capacity evaluation," *IEEE Journal on Selected Areas in Communications*, vol. 32, no. 6, pp. 1164-1179, June 2014.
- [2] X. Wu et al., "60-GHz Millimeter-Wave Channel Measurements and Modeling for Indoor Office Environments," *IEEE Transactions on Antennas and Propagation*, vol. 65, no. 4, pp. 1912-1924, April 2017.
- [3] J. Zhu, H. Wang and W. Hong, "Characterization of large-scale fading for 45 GHz indoor channels," in *3rd Asia-Pacific Conference on Antennas and Propagation*, Harbin, 2014, pp. 728-730.
- [4] S. Salous, N. Nikandrou and N. F. Bajj, "Digital techniques for mobile radio chirp sounders," *IEE Proceedings - Communications*, vol. 145, no. 3, pp. 191-196, June 1998.

- [5] C. U. Bas et al., "A Real-Time Millimeter-Wave Phased Array MIMO Channel Sounder," in *2017 IEEE 86th Vehicular Technology Conference (VTC-Fall)*, Toronto, 2017, pp. 1-6.
- [6] W. Keusgen, A. Kortke, M. Peter and R. Weiler, "A highly flexible digital radio testbed and 60 GHz application examples," in *2013 European Microwave Conference*, Nuremberg, 2013, pp. 740-743.
- [7] E. Zöchmann et al. "Measured Delay and Doppler Profiles of Overtaking Vehicles at 60 GHz," in *12th European Conference on Antennas and Propagation*, London, 2018, pp. 1-5.
- [8] S. Sangodoyin, J. Salmi, S. Niranjayan and A. F. Molisch, "Real-time ultrawideband MIMO channel sounding," in *6th European Conference on Antennas and Propagation (EUCAP)*, Prague, 2012, pp. 2303-2307.
- [9] T. S. Rappaport, "Characterization of UHF multipath radio channels in factory buildings," *IEEE Transactions on Antennas and Propagation*, vol. 37, no. 8, pp. 1058-1069, Aug. 1989.
- [10] A. Chandra, J. Blumenstein, T. Mikulášek, J. Vychodil, R. Maršálek, A. Prokeš, T. Zemen, C. A. Mecklenbräuker, "Serial subtractive deconvolution algorithms for time-domain ultra wide band in-vehicle channel sounding," *IET Intelligent Transport Systems*, vol. 9, no. 9, pp. 870-880, Nov. 2015.
- [11] G. R. MacCartney, Jr. and T. S. Rappaport, "A Flexible Millimeter-Wave Channel Sounder with Absolute Timing," *IEEE Journal on Selected Areas in Communications*, vol. 35, no. 6, pp. 1402-1418, June 2017.
- [12] R. Zhang, S. Wang, X. Lu, W. Duan and L. Cai, "Two-Dimensional DoA Estimation for Multipath Propagation Characterization Using the Array Response of PN-Sequences," *IEEE Transactions on Wireless Communications*, vol. 15, no. 1, pp. 341-356, Jan. 2016.
- [13] A. Prokes, J. Vychodil, M. Pospisil, J. Blumenstein, T. Mikulasek and A. Chandra, "Time-domain nonstationary intra-car channel measurement in 60 GHz band," 2016, in *International Conference on Advanced Technologies for Communications (ATC)*, Hanoi, 2016, pp. 1-6.
- [14] R. Zetik, M. Kmec, J. Sachs, and R. S. Thomä, "Real-Time MIMO Channel Sounder for Emulation of Distributed Ultrawideband Systems," *Int. J. Antennas Propag.*, vol. 2014, Article ID 317683, pp. 1-16, 2014.
- [15] G. R. MacCartney, Jr. and T. S. Rappaport, '5G mmWave Channel Sounder', 2017. [Online]. Available: <https://wireless.engineering.nyu.edu/mmwave-5g-channel-sounder/>. [Accessed: 10- Jun- 2018].
- [16] D. Ferreira, R. F. S. Caldeirinha and N. Leonor, "Real-time high-resolution radio frequency channel sounder based on the sliding correlation principle," *IET Microwaves, Antennas & Propagation*, vol. 9, no. 8, pp. 837-846, June 2015.
- [17] J. Vychodil, M. Pospisil, A. Prokes, J. Blumenstein, "Millimeter Wave Band Time Domain Channel Sounder," *IET Communications*. Accepted for publication.
- [18] 'FC1005V/00 V-band Converter with LO'. [Online]. Available: <https://www.siversima.com/wp-content/uploads/FC1005V00-Data-Sheet.pdf>. [Accessed: 15- Jun- 2018].
- [19] 'LPRO Rubidium Oscillator for Time & Frequency Reference. User's guide and integration guidelines', [Online]. Available: <http://www.ham-radio.com/sbms/LPRO-101.pdf>. [Accessed: 18- May- 2017].
- [20] T. Mikulasek, J. Blumenstein, and A. Prokes, "Antennas utilized for intra-vehicle 3-11 GHz and 55-65 GHz channel measurement," in *37th PIERS*, Shanghai, 2016, pp. 1-5.
- [21] M. Golay, "Complementary series," *IRE Transactions on Information Theory*, vol. 7, no. 2, pp. 82-87, Apr. 1961.
- [22] J. Vychodil, A. Chandra, T. Mikulasek, A. Prokes and V. Derbek, "UWB time domain channel sounder," in *Radioelektronika*, Pardubice, 2015, pp. 268-271.
- [23] S. A. Billings, S. Y. Fakhouri, "Identification of non-linear systems using correlation analysis and pseudorandom inputs," *International Journal of Systems Science*, vol. 11, no. 3, pp. 261-279, Jan. 1980.
- [24] 'MSO/DPO70000 Series Digital and Mixed Signal Oscilloscopes Datasheet', 2016. [Online]. Available: <http://www.tek.com/datasheet/mso-dpo70000-series-digital-and-mixed-signal-oscilloscopes-datasheet>. [Accessed: 15- Jun- 2018].
- [25] R. J. Polge and E. M. Mitchell, "Impulse Response Determination by Cross Correlation," *IEEE Transactions on Aerospace and Electronic Systems*, vol. AES-6, no. 1, pp. 91-97, Jan. 1970.